Multiscale Laboratory Mechanical Performance of SDA Mixtures with Construction and Demolition Waste Filler

Peter Mikhailenko[1]; Martin Arraigada[2]; Zhengyin Piao[3]; and Lily D. Poulikakos[4]

Abstract: The incorporation of waste materials into road materials provides an excellent opportunity for partial reductions in virgin material consumption while providing a valuable alternative destination for the would-be waste. However, the incorporation of these materials and the performance limitations of the resulting asphalt need to be carefully examined, especially with regards to the asphalt cracking susceptibility. The current study focuses on the use of construction waste fillers as partial aggregate replacement in semidense asphalt (SDA) mixtures. Both concrete waste in the form of recycled concrete aggregates (RCA) and mixed construction and demolition (C&D) waste are examined. The indirect tensile (IT) stiffness modulus was found to not be affected significantly by the filler replacement. The IT fatigue resistance was found to be somewhat lower with the waste material using the classical approach, but similar when looking at the damage rate. In addition to the smaller-scale testing, larger-scale testing was conducted on the control and RCA filler mixtures using the Mobile Model Load Simulator (MMLS3), and similar cracking resistance was found for both mixtures while advancing a novel crack length measurement method using digital image correlation. The results showed that the incorporation of RCA filler into semidense asphalt mixtures is a viable solution reducing the need for virgin filler. **DOI: 10.1061/(ASCE)MT.1943-5533.0004244.**

Author keywords: Model Mobile Load Simulator; Semidense asphalt (SDA); Stiffness modulus; Fatigue; Cracking.

Introduction

Construction and demolition (C&D) waste is the largest source of waste materials in industrialized regions such as Europe. Within the C&D waste, waste concrete accounts for a considerable fraction (Monier et al. 2011). By means of mechanical processing, the waste concrete is converted into recycled concrete aggregate (RCA) as a secondary raw material, which can be further used by the industry such as with concrete production (Marie and Quiasrawi 2012). Nevertheless, there is still a gap between the full reuse of RCA and current condition in the European countries. For example, around 15% of RCA is not reused and does not go into the recycling stream in Switzerland, resulting in stacking or landfilling (Gauch et al. 2016). This number can be as high as 46% for European Union countries (Monier et al. 2011). One of the reasons is that the fine RCA is generally not recommended as the raw material for producing new concrete due to its high water absorption (Nedeljković et al. 2021). As a result, the recycling of RCA within a fully closed loop still cannot be achieved. To overcome the current challenge, it is important to explore other destination industries for RCA.

Asphalt mixtures are the most important and widely used road material, with an annual production of nearly 300 Mt in Europe (EAPA 2018). Asphalt mixtures are composed of more than 90% of aggregates of various sizes, requiring a considerable consumption of quarried stone. As a result, the idea of using waste aggregates is proposed to reduce the requirement of virgin raw materials and stimulate the recycling of waste. Among various waste materials, RCA is one of the candidates with potential to be used in asphalt mixtures (Piao et al. 2021).

Several studies have investigated RCA as the coarse and fine aggregates of dense asphalt pavement (Albayati et al. 2018; Arabani and Azarhoosh 2012; Kareem et al. 2018; Ossa et al. 2016). However, these studies drew different conclusions on the mechanical performance of asphalt mixtures with RCA. For example, Albayati et al. (2018) reported that the moisture resistance of asphalt mixtures can be improved by using RCA to replace 20% of the coarse aggregate, but opposite results were found by Kareem et al. (2018). Arabani and Azarhoosh (2012) indicated that the replacement of fine aggregate by RCA can improve the fatigue resistance of asphalt mixtures, whereas negative conclusions were drawn by Wu et al. (2017). These conflicts can be attributed to several factors such as different binder type, binder content, and RCA quality. Regarding filler replacement, Chen et al. (2011) investigated the use of RCA powder in dense asphalt. Their results showed that the mechanical performance (resistance to rutting, moisture, and fatigue) of asphalt mixtures can be improved by RCA filler.

[1]Concrete and Asphalt Laboratory, Empa—Swiss Federal Laboratories for Materials Science and Technology, Überlandstrasse 129, Dübendorf 8600, Switzerland (corresponding author). ORCID: https://orcid.org/0000-0001-6359-2937. Email: peter.mikhailenko@empa.ch

[2]Concrete and Asphalt Laboratory, Empa—Swiss Federal Laboratories for Materials Science and Technology, Überlandstrasse 129, Dübendorf 8600, Switzerland. ORCID: https://orcid.org/0000-0001-8435-7565. Email: martin.arraigada@empa.ch

[3]Concrete and Asphalt Laboratory, Empa—Swiss Federal Laboratories for Materials Science and Technology, Überlandstrasse 129, Dübendorf 8600, Switzerland; ETH Zurich, Swiss Federal Institute of Technology Zurich, Institute of Environmental Engineering, Ecological Systems Design, John-von-Neumann-Weg 9, Zurich 8093, Switzerland. Email: zhengyin.piao@empa.ch

[4]Concrete and Asphalt Laboratory, Empa—Swiss Federal Laboratories for Materials Science and Technology, Überlandstrasse 129, Dübendorf 8600, Switzerland. ORCID: https://orcid.org/0000-0002-7011-0542. Email: lily.poulikakos@empa.ch

Note. This manuscript was submitted on June 29, 2021; approved on October 21, 2021; published online on March 23, 2022. Discussion period open until August 23, 2022; separate discussions must be submitted for individual papers. This paper is part of the ***Journal of Materials in Civil Engineering***, © ASCE, ISSN 0899-1561.

Table 1. Properties of aggregates

Aggregate source	Size	Apparent density (kg/m^3)	Relative density (kg/m^3)	WA_{24} (%)
Control	2/4 mm	2,693	2,644	0.69
Control	Filler	2,719	2,696	0.32
Control	0.1/4 mm	2,650	—	—
RCA	2/4 mm	2,677	2,308	5.97
RCA	Filler	2,669	—	—
C&D	Filler	2,658	—	—

Note: WA_{24} = 24-h water absorption using EN 1097-6.

Apart from the dense asphalt, previous studies replaced RCA in the coarse aggregate, sand, and filler of semidense asphalt (SDA) mixtures (Mikhailenko et al. 2020a, 2021). SDA has an elevated air voids content in comparison with that of dense asphalt and porous asphalt. In Switzerland and several European countries, SDA is applied as a type of low-noise pavement (Mikhailenko et al. 2020b), considering its balance of acoustic and mechanical performance (Bühlmann and Hammer 2017). Because SDA requires high-quality aggregate to ensure durability, it would be challenging to incorporate recycled materials in SDA. This can be found in the results of Mikhailenko et al. (2020a), which showed that the RCA coarse aggregate and sand replacement led to improved rutting resistance but also higher moisture sensitivity and binder absorption. However, the RCA filler showed the same performance in moisture sensitivity and rutting tests to that of the control filler, implying the use of RCA filler in SDA to be promising.

Following the work of Mikhailenko et al. (2020a, 2021), this article continues the investigation of SDA with RCA and mixed C&D fillers and focuses on the stiffness, fatigue, and resistance to cracking of the mixtures at intermediate and large laboratory scales. The stiffness and fatigue resistance of the mixtures were evaluated by cyclic indirect tensile loading, and Model Mobile Load Simulator (MMLS3) was used to simulate the bottom-up crack initiation and propagation in asphalt pavements at a laboratory scale using slab samples. The MMLS3 cracking tests were combined with deflection measurements and digital image correlation (DIC) to observe the crack development of the asphalt mixtures, where a method for measuring the crack length using the DIC was developed.

Materials and Experimental Design

Materials

Bitumen

From the requirements for SDA in Switzerland [SN 640 436 (Swiss Standard 2013)], the bitumen was styrene-butadienestyrene (SBS) polymer-modified binder (PMB), penetration graded at 45/80–65 according to EN 1426 (CEN 2015).

Aggregates

The mixture aggregates, including the filler, were quarried sandstone from Massongex, Switzerland. The RCA aggregates and filler were from concrete plant waste from the excess of various mixes from the Canton of Zurich, Switzerland, region and contained a variety of different minerals. The bulk RCA was sieved to attain the filler and appropriate coarse aggregates (gradation of 2/4 mm), with the latter being washed to remove the fines. The C&D filler was sieved from bulk C&D waste collected from various demolition sites in the Canton of Zurich area. The apparent and relative aggregate densities were determined by EN 1097-6 (CEN 2013) (by gas pycnometer for the fillers) and are provided in Table 1, where it can be seen that the filler densities are similar for the three types. The RCA coarse aggregate differs from the control in having a lower density and higher water absorption.

Asphalt Mixtures

The semidense asphalt (SDA 4-12) tested in this study is a common mixture in Switzerland used due to its properties as a low-noise pavement (SN 640 436), with a maximum aggregate size of 4 mm and a target voids content of 12% ± 2%. In addition to the control mixture, mixtures replacing the control filler with RCA filler and C&D waste filler (FL) by volume were produced. Additionally, a mixture incorporating RCA coarse-aggregate replacement, at about 10% of the total aggregate volume was also tested (RCA Max). This mixture aimed to maximize the total RCA replacement based on previous findings (Mikhailenko et al. 2020a). The mixture designs are given in Table 2, and the gradations in Fig. 1, where it can be seen that the gradations are almost the same.

The mixture was produced by heating the aggregates and bitumen to 170°C. The aggregates were mixed on their own for 5 min, after which the bitumen was added followed by another 5 min of mixing. The maximum relative density of the loose mixtures were determined according to EN 12697-5 (CEN 2019).

Compaction and Sample Preparation

All of the mixtures were short-term aged by placing the loose mix in a forced draft oven for 2 h at the compaction temperature of 155°C. The asphalt samples for the stiffness modulus and fatigue tests were compacted using gyratory compaction at 155°C. The cylindrical samples were compacted to around 16% air voids, a diameter of 99.5 ± 0.5 mm, and a height of 62 ± 2 mm, estimating based on previous experience that the cut samples from the middle of the specimen would have a voids content of around 12%. About 10 mm were cut from the top and bottom of the samples, bringing their height to 42 ± 2 mm. The density and air voids of the samples were then determined geometrically according to EN 12697-29 (CEN 2002).

For the MMLS3 crack initiation and propagation tests, slab-shaped samples with a dimension of 1.6 m long, 0.6 m wide, and a thickness of 0.04 m were compacted with an unheated metal roller drum until reaching the required height for the desired air voids of around 12% (Fig. 2). Due to the difficulty to maintain

Table 2. Asphalt mixture designs by percent of mass

		Control fraction (%)			Waste fraction (%)			Binder (%)
Mixture	Code	2/4	0.125/4	Filler	RCA 2/4	RCA FL	C&D FL	PMB 45/80–65
Control	Cont	62.8	23.8	7.2	—	—	—	6.1
RCA filler	RCAFL	62.9	23.9	—	—	7.0	—	6.1
RCA filler +10%2/4	RCA Max	53.4	24.1	—	8.8	7.2	—	6.5
C&D filler	CDFL	62.9	23.9	—	—	—	7.0	6.1

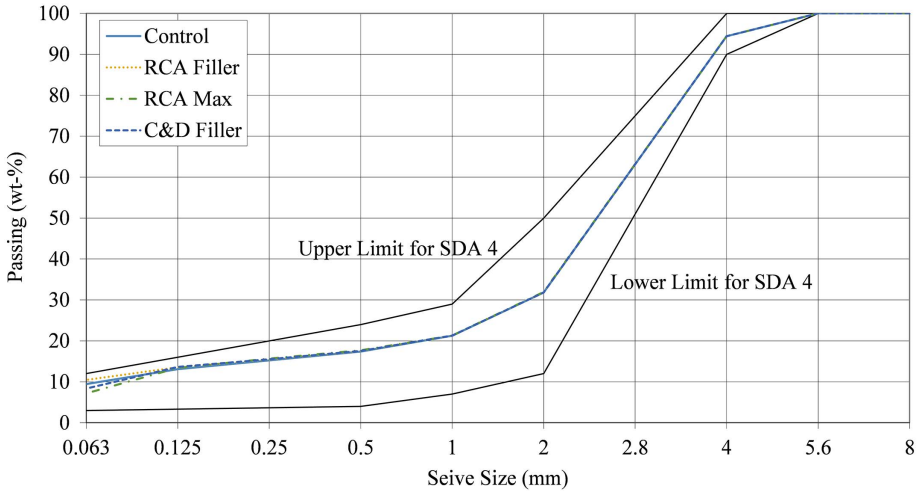

Fig. 1. Gradations of mix designs within the limits for SDA 4 in Swiss standard SN 640 436.

the compaction temperature for such a large area, the average temperature during the compaction was measured to be around 90°C–110°C. After the MMLS3 cracking tests, 100-mm-diameter cores were extracted from the slabs, and the air voids determined according to EN 12697-29. The absorbed and effective asphalt binder content were estimated based on Superpave guidelines (McGennis et al. 1995).

Experimental Design

Cyclic Indirect Tensile Stiffness Modulus

The stiffness modulus was obtained according to the TP Asphalt-StB Part 25 B 1 guidelines established by the German Road and Transportation Research Association using the indirect tensile (IT) setup with sinusoidal cyclic loading (FGSV 2009). The horizontal deformation was measured by LVDTs on either side of the sample. The sinusoidal loading frequencies were 0.1, 1, and 10 Hz conducted at temperatures of 5°C, 10C, and 15°C. First, the load amplitude required for 75 $\mu\varepsilon$ deformation for each mixture at each temperature and frequency was determined. Subsequently, the loading of each sample was conducted, testing four specimens per mixture. The horizontal stress is calculated from the force (F) reading based on Eq. (1)

Fig. 2. Roller compaction of 1.6 × 0.6 × 0.04-m slab for MMLS3 test.

$$\sigma = \frac{2F}{\pi \times d \times h} \tag{1}$$

where h = sample height; and d = sample diameter. From the stress, the stiffness modulus ($|E|$) of the samples could be calculated according to Eq. (2)

$$|E| = \frac{\Delta F \times (0.274 + \mu)}{h \times \Delta u} \tag{2}$$

where ΔF = difference between maximal and minimal force from the sinusoidal loading; μ = Poisson's ratio of the material at the temperature (assumed 0.239 at 10°C from FGSV 2009); h = sample height; and Δu = difference between the maximal and minimal displacement (Poulikakos et al. 2014).

Cyclic Indirect Tensile Fatigue Resistance

The fatigue resistance of the samples was tested according to TP Asphalt-StB Part 25 B 1 (FGSV 2009), using the IT setup as for the stiffness modulus, with cyclic, sinusoidal, and stress-controlled loading. The mixtures were tested at three strains corresponding to 20,000–1 million cycles of fatigue life, with three samples for each strain per mixture.

The failure criteria was based on the energy ratio (ER) concept, taken as the stiffness modulus (discussed in the preceding section) multiplied by the number of cycles ($|E| \times N$). The failure (N_f) is taken as the number of cycles where the ER has reached its maximum (Fig. 3). The maximum applied stress level corresponding to 1 million cycles (σ_6) was determined by plotting log N_f versus the log of the maximum applied stress per cycle (log σ_i). This was compared with ε_{ini6}, which was calculated by plotting the log N_f versus the log of the initial strain (log ε_{ini}), which was taken as the average for the first 100 cycles.

Finally, a simplified analysis of the damage rate (Fig. 4) was performed based on previous work (Di Benedetto et al. 2004). Here, the heating bias effects found in the loss of modulus was not considered. The total damage rate (a_{Ti}) was taken as the slope of the decrease in $|E|$ versus cycles (N) [Eq. (3)], normalized by the intercept of the slope at $N = 0$ (E_{0i})

$$a_{Ti} = \frac{d|E|_i/dN_i}{E_{0i}} \tag{3}$$

The damage rate was taken at the following intervals based on the results, and it was only taken when they could clearly be

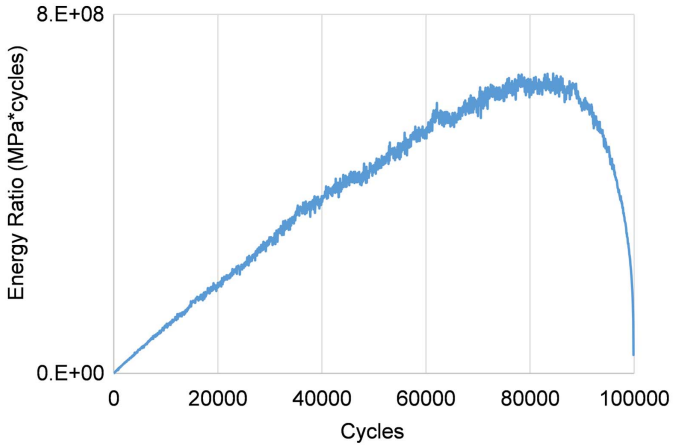

Fig. 3. Energy ratio and finding N_f for typical fatigue test.

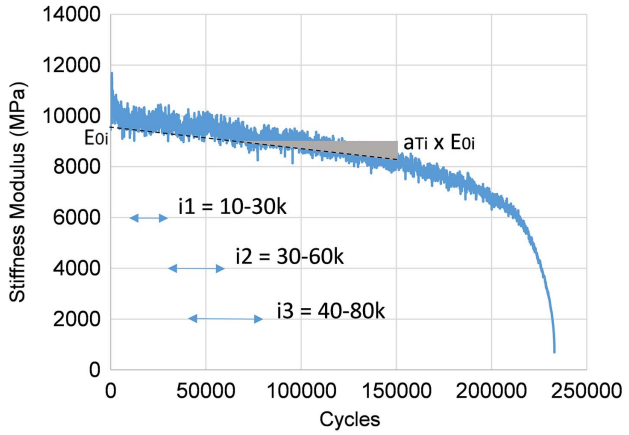

Fig. 4. Calculation of damage rates from fatigue test.

identified in the steady loading phase and not in the rapid failure phase (see "MMLS3 Cracking Tests" section:

- Interval $i = 1$ from 10,000 to 30,000 cycles,
- Interval $i = 2$ from 30,000 to 60,000 cycles, and
- Interval $i = 3$ from 40,000 to 80,000 cycles.

MMLS3 Cracking Tests

MMLS3 was used to validate the laboratory results obtained on cylindrical specimens (Zaumanis et al. 2019). The MMLS3 is a downscaled traffic simulator with four pneumatic wheels that load the pavement with around 7,200 unidirectional wheel passes per hour over a length of about 1.2 m (Fig. 5). The design of the machine is such that only one wheel is touching the pavement at a time at a speed of about 9 km/h. The height of the device can be adjusted so each wheel is able to apply a load of about 2.1 kN. This type of test uses rolling wheels to induce damage in asphalt slabs, similar to the way that traffic deteriorates pavements (Arraigada et al. 2014). Depending on the temperature of the slab, it can also be used to study the rutting or cracking performance.

For this work, four slabs were loaded until total crack failure (slab cracked from the bottom to the top surface) at an air temperature of 20°C ± 2°C. Two of the slabs were prepared using SDA with filler replacement (RCAFL), and the other two were made of conventional SDA as the control specimens. In order to induce the formation of a crack, the 4-cm-thick slabs had a 1-cm notch perpendicular to the traffic direction in the middle of the bottom surface. This ensured that fatigue induced crack developed at the center of the sample, where its progress could be monitored. The slabs were laid on top of a rubber mat that simulated the relative weaker support of the subgrade (Fig. 5). Furthermore, the slabs were supported by two aluminum profiles on the rear and front edges to facilitate bending under load. Schematically, the configuration could be represented as a simply supported beam on an elastic foundation simulating typical flexible pavements, with fatigue-induced bottom-up crack growth.

In order to monitor the crack development, LVDTs were installed close to the edge along the span of the sample to measure

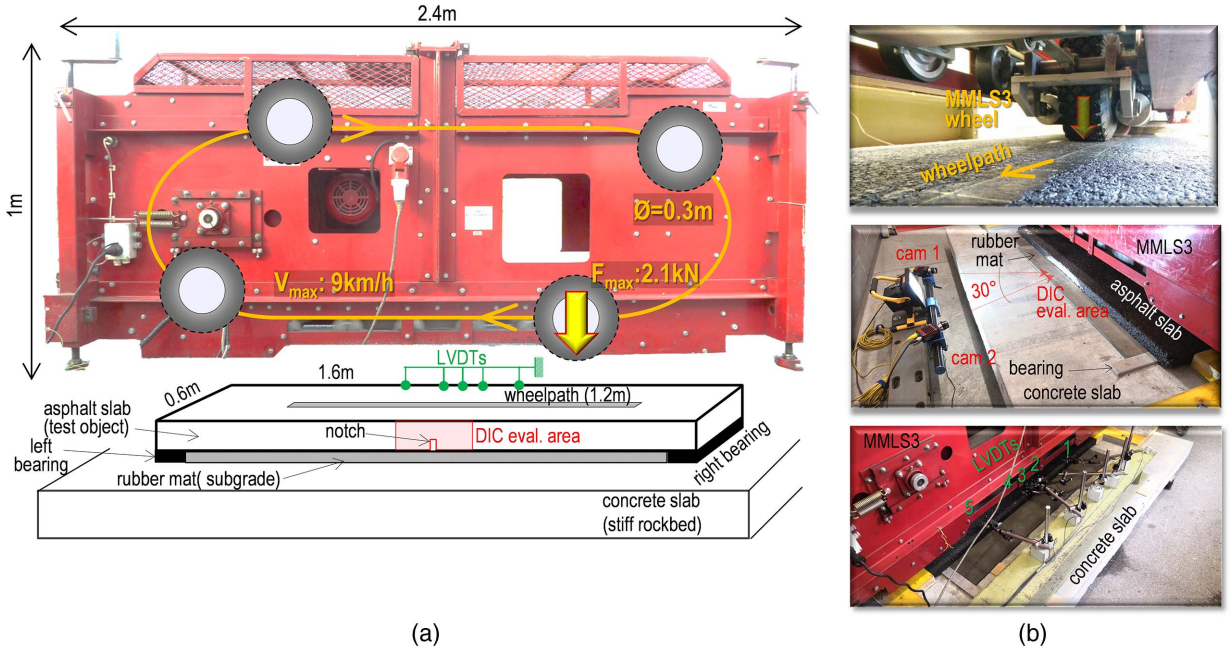

Fig. 5. (a) MMLS3 cracking test setup; and (b) load application area, DIC system, and LVDT measuring arrangement.

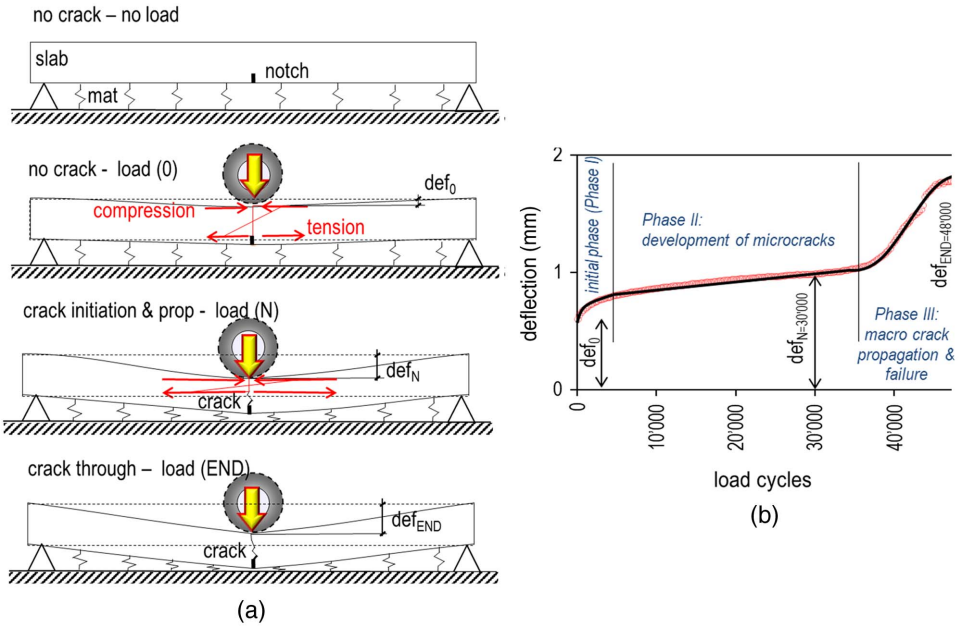

Fig. 6. (a) Schematic concept of the MMLS3 test progression; and (b) typical evolution of deflection.

the deflection of the slab during loading. A LVDT was placed in the middle of the span, two LVDTs 10 mm from the center on either side, and another two LVDTs 40 mm from the center. The deflection was periodically recorded to indirectly determine the cracking development according to different phases of the deflections versus load application curves, as shown in the right side of Fig. 6. In this calculation, deflection (def) is defined as the difference between the LVDT reading when a wheel is passing over the sensor (i.e., maximum vertical deformation) and when none of the MMLS3 wheels are touching the slab (i.e., the slab is not loaded). As shown in Fig. 6(a), the deflection will increase with the accumulation of MMLS3 load applications. A certain initial value def_0 will increase to a final value def_{END} when a fatigue crack progresses from the bottom to the top of the slab. Ideally, three phases that can be correlated to the damage progression.

After an initial phase where the deflections increase due to the adjustment of the system to the loads in Phase I, a steady state smooth increase in Phase II [Fig. 6(b)] is an indicator of the development of microcracks invisible to the naked eye. The sudden deflection increase of the Phase III is a sign that a macrocrack started in the notch and travels through the thickness of the slab until it totally fails and splits in two pieces.

In addition to the measurement of deformation, the crack development was monitored by DIC. This noncontact optical technique measures the deformation of a body under load by tracking and connecting the displacements of random speckle patterns applied to its surface. The lateral surface around the notch, about 15 cm in each direction, was grinded to make it smooth. A white dot speckle pattern was sprayed with a high-pressure nozzle for better pixilation (Fig. 7). Two cameras placed at an angle of about 30° and pointing at the notch monitored this area. Image recording was triggered periodically, approximately every1,200 MMLS3 load cycles. Each image recording comprised 50 frames taken in a 2-s window, i.e., enough to capture the passing of the MMLS3 wheels with a sampling rate of 25 Hz. The software used for the measurement and the post-processing of the images was the Istra4D 4.4.2, which allowed to measure the crack length development at the center of the sample. In order to detect a crack, images of the nonloaded state (when no wheel is touching the slab) were compared with the loaded state.

An example of the crack detection process used in this work is presented in Fig. 7. In a noncracked surface, there is a monochromatic distribution as there is no discontinuity in the deformation field. When a crack is present, there is a clear discontinuity. Once the crack propagates further, more color distinctions are possible. If the image is further enhanced by reducing the color pallet range to 0.0005–0.0015 mm around the crack, the color spectrum results in a thin line following the crack length, which discontinues at the tip (Fig. 8). From here, the vertical crack length can be manually estimated measuring the linear distance between the crack start and tip. In order to be able to compare the different results the timestamps of the DIC images, the LVDT measurements and loading cycles were carefully synchronized.

Results

Volumetric Properties of the Mixtures

The air voids content as well as the estimated absorbed/effective binder contents are found in Table 3. The average air void contents are similar but up to 0.5% higher on average than for the control. The effective binder contents are very similar, indicating a correct amount of extra binder was added to the mixture containing 10% RCA 2/4.

Cyclic Indirect Tensile Stiffness Modulus

The stiffness modulus results are shown in Fig. 9. For all of the different temperatures and frequencies, the mixtures with RCA coarse-aggregate replacement and filler (RCA Max) have the highest stiffness. The mixture with C&D waste filler has similar stiffness to the control, whereas the RCA filler seems to be lower for all of the mixtures. However, at most temperatures and frequencies, the differences between the mixtures are within or very close to the range of the standard deviation, indicating very similar performance overall.

J. Mater. Civ. Eng., 2022, 34(6): 04022106

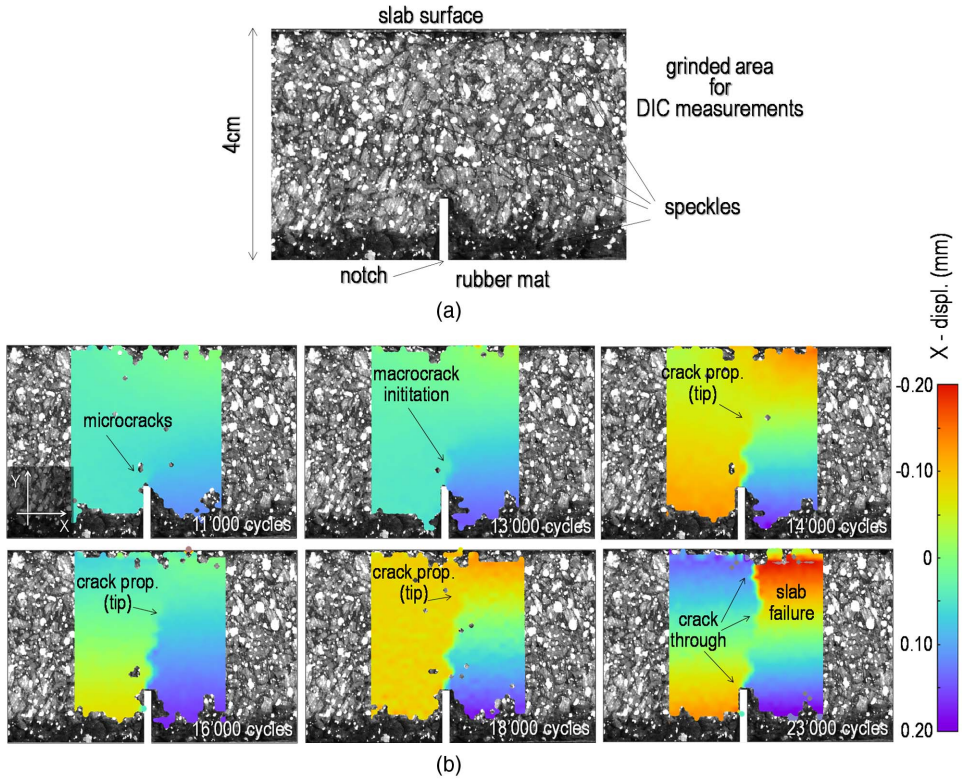

Fig. 7. Example of the DIC measurements: (a) view of the speckled DIC area; and (b) results of different damage phases of slab RCAFL 2 with respect to number of cycles.

Cyclic Indirect Tensile Fatigue Resistance

As discussed in the previous section, the modulus during the fatigue tests is gradually reduced until failure. In order to produce a fatigue analysis, a minimum of nine repetitions is needed at three strain/stress levels. The results were analyzed based on the Wohler curve stress/strain at 1 million cycles as well as the damage rate. The analysis of the stress (σ_6) and strain (ε_6) levels at 1 million cycles is shown in Figs. 10 and 11, respectively, and the values are given in Table 4. The strains used to calculate ε_6 were based on the average strain for the initial hundred cycles. The results from both values indicated that the samples with the waste materials were less resistant to fatigue than the control. Both σ_6 and ε_6 show fairly high R^2 values.

The damage rate for the intervals of 10,000–30,000, 30,000–60,000, and 40,000–80,000 cycles are shown in Figs. 12–14, respectively. The slopes of the lines indicate that the samples' performance was much closer than the fatigue curves in Figs. 10 and 11 indicated. However, these results had a significant amount of scatter.

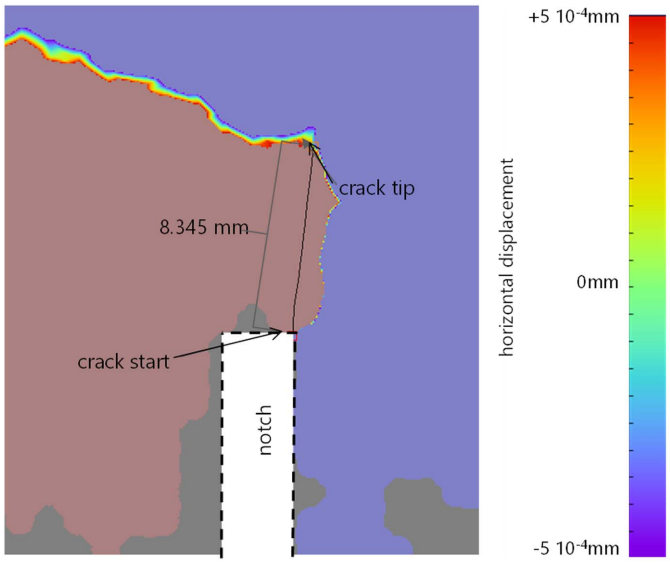

Fig. 8. Example of crack length estimation for RCAFL 2 sample at around 12,000 cycles.

MMLS3 Cracking Tests

Fig. 15 shows the increase of deflection amplitudes in the center of the four tested slabs during the loading with MMLS3. These included two slabs from the control, two from RCAFL, and the best performing waste mixture in the smaller scale tests. These deflections are relative to the initial values, i.e., they have been shifted so they are at zero at the beginning of the loading.

Table 3. Volumetrics of gyratory-compacted stiffness/fatigue samples

Mixture	Air voids (%)	Absorbed binder (%)	Effective binder (%)
Control	12.8	0.6	5.5
Standard deviation	0.2	—	—
RCAFL	13.0	0.3	5.8
Standard deviation	0.3	—	—
RCA max	13.3	0.8	5.8
Standard deviation	0.2	—	—
CDFL	13.2	0.2	5.9
Standard deviation	0.3	—	—

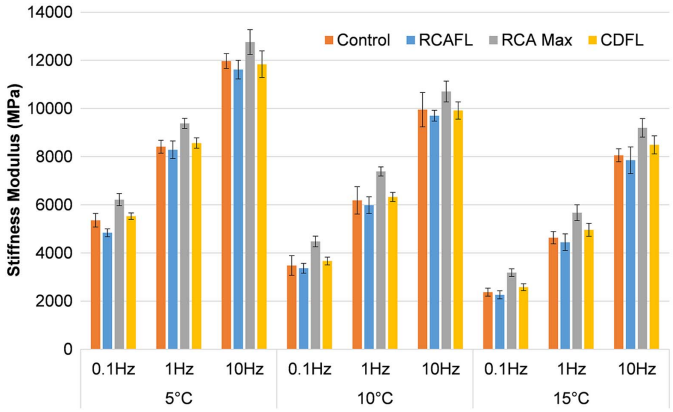

Fig. 9. Stiffness modulus at different temperatures and frequencies.

Table 4. Stress (σ_6) and strain (ε_6) levels to 1 million fatigue cycles

Sample	σ_6 (MPa)	R^2	ε_6 (μm/m)	R^2
Control	0.406	0.98	683.9	0.89
RCA filler	0.381	0.92	632.1	0.91
RCA max	0.371	0.93	605.3	0.96
C&D filler	0.337	0.95	586.3	0.98

Table 5. Approximate number of MMLS3 load cycles to reach crack initiation and slab failure

	Load cycles	
Sample	Macrocrack initiation	Slab failure
Control 1	13,000	23,000
Control 2	10,800	19,000
RCAFL 1	10,000	19,000
RCAFL 2	13,000	21,000

From the damage progression curves it is possible to identify the different cracking phases [Fig. 6(b); Table 5] by looking at how the slopes change. Here, the control and RCAFL samples showed the same performance, with the difference between the two mixtures not being more than between samples of the same mixture. These differences can be attributed to variability between the samples rather than a difference in the performance of the mixtures, with the variability within the range found previously (Zaumanis et al. 2020) being due to the sample compaction on a larger scale and corresponding to a higher performance range in the field.

The analysis of the DIC images and estimated crack lengths (Fig. 16) showed that the cracking started at around 5,000–9,000 cycles. The development of the crack length starts with a

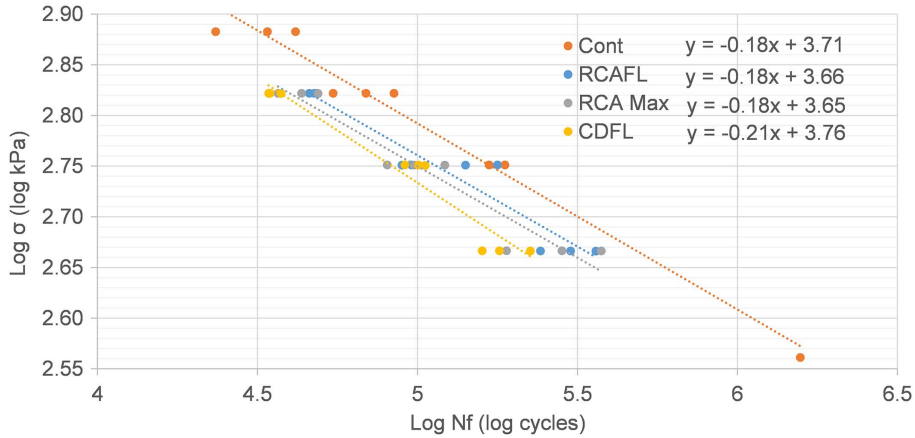

Fig. 10. Stress versus cycles to failure for fatigue.

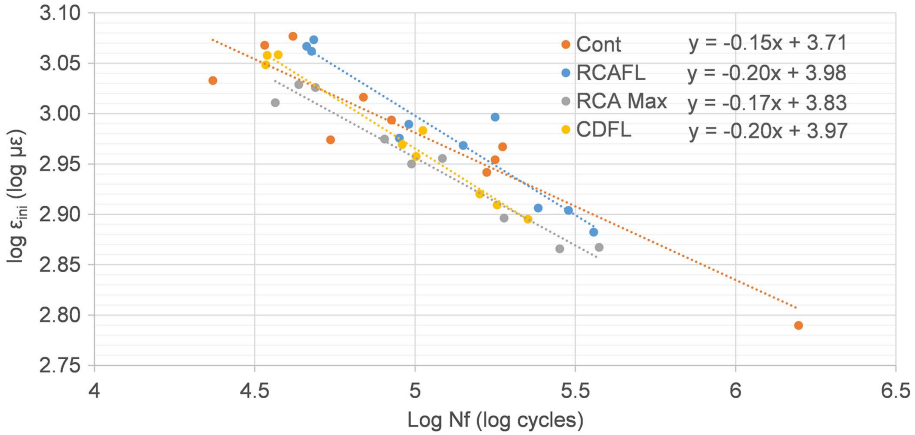

Fig. 11. Initial strain versus cycles to failure for fatigue.

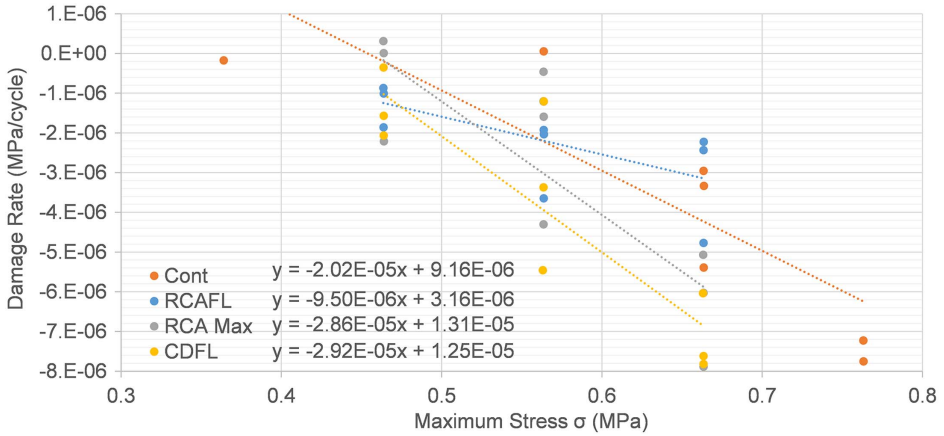

Fig. 12. Fatigue damage rate at 10,000–30,000 cycles.

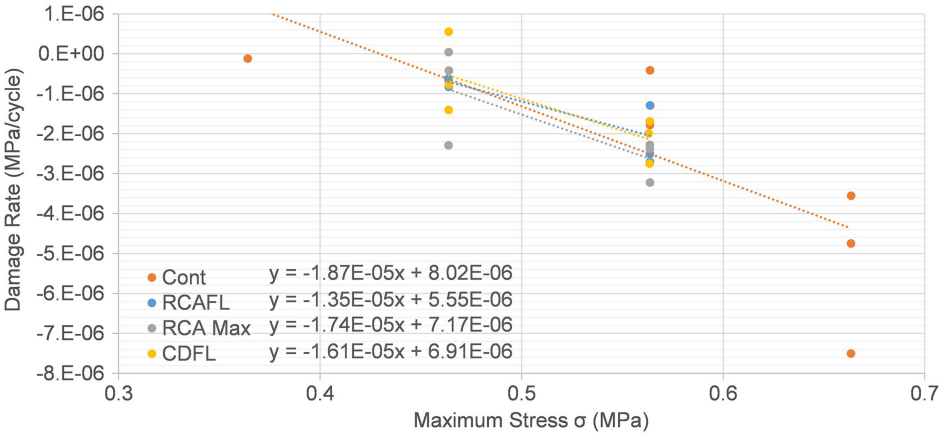

Fig. 13. Fatigue damage rate at 30,000–60,000 cycles.

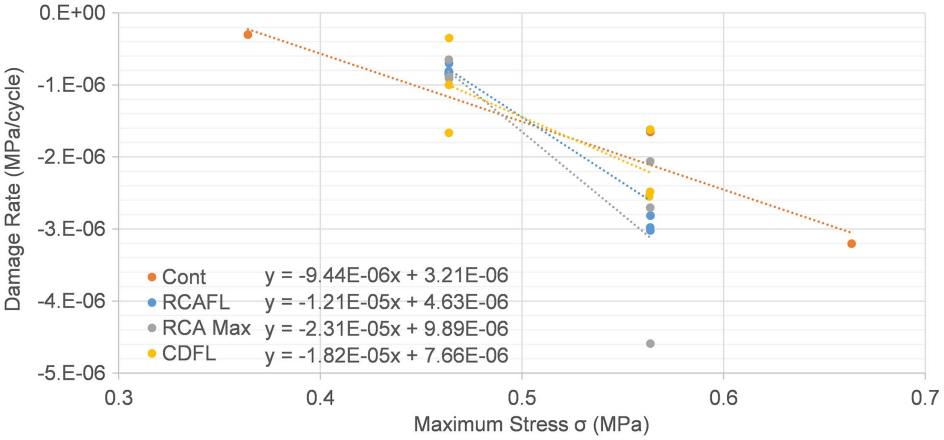

Fig. 14. Fatigue damage rate at 40,000–80,000 cycles.

lower slope, increasing rapidly at a certain inflection point. This inflection also occurs after the vertical deflection, but with a few hundred cycles of lag compared with the estimated crack length.

The development of the deformation (Fig. 16) follows a relatively constant increase until after 10,000 cycles, where the slope of the graph significantly decreases. The middle region of the graph can be considered Phase II, where the cracking is initiated, whereas the region after 10,000 cycles can be considered Phase III, where crack propagation and failure takes place (Di Benedetto et al. 2004). Complete failure, defined as the moment when the crack reaches the surface of the slab, was in the region of the 20,000 cycles. An overview of these estimated values for each slab is presented in Table 3.

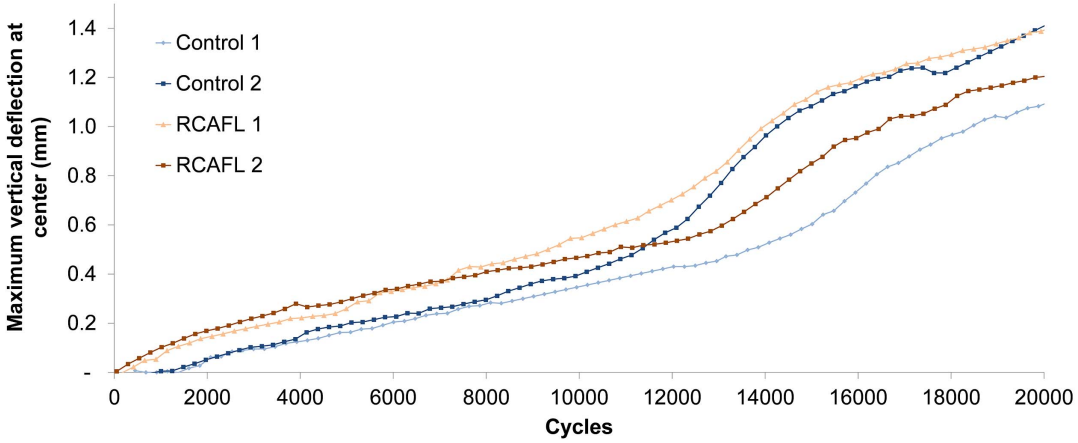

Fig. 15. MMLS3 maximum vertical deformation at middle versus number of cycles.

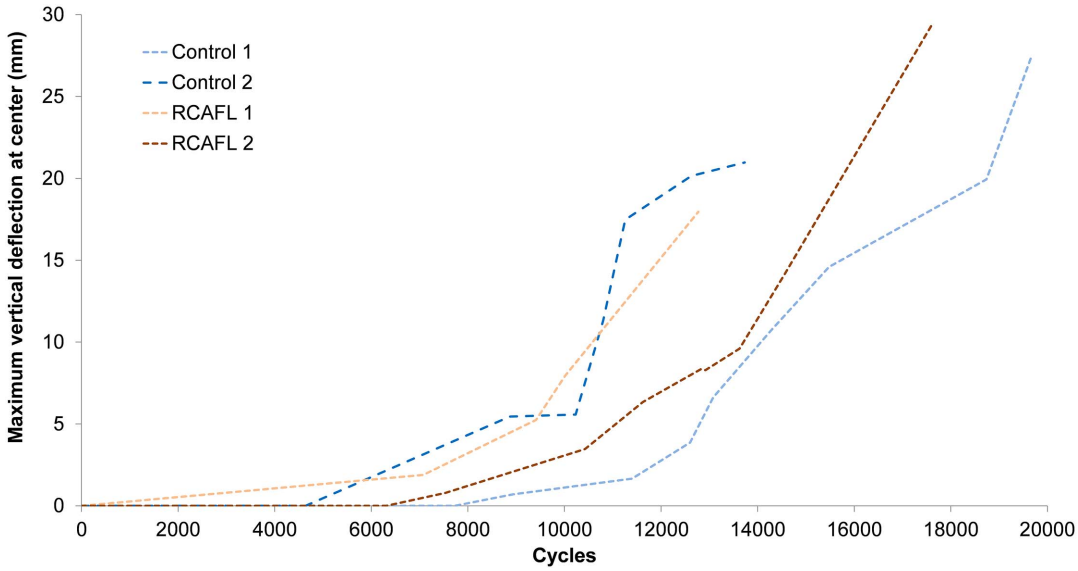

Fig. 16. MMLS3 estimated crack length based on DIC versus number of cycles.

Discussion

Investigating the material at intermediate scales (100-mm cylinders), the mechanical properties of SDA waste filler replacement were evaluated using stress-controlled IT stiffness modulus and fatigue tests. The stiffness modulus of the waste mixtures were compared with that of the control, and it was found that the mixture with 10% RCA coarse aggregate consistently had the highest stiffness values. This confirms previous findings and is attributed to the rougher surface of coarse RCA compared with the control (Mikhailenko et al. 2021), causing stronger interaggregate contact and increased resistance to loading. The C&D filler did not have an effect on the stiffness, whereas the RCA filler on its own, on the other hand, seemed to reduce the stiffness compared with the control.

Investigating the material at a larger laboratory scale using the MMLS showed that deformation of the slabs was similar in performance with the control and RCA filler mixtures. This seems to contradict previous findings showing no or very little effect on the stiffness (Chen et al. 2011; Mikhailenko et al. 2020a).

The fatigue results showed a somewhat lower fatigue for all of the waste material samples compared with the control. This was clearer when looking at the applied stress than with the strain and damage rate, where the difference between the mixtures is not apparent. When taking the σ_6 values, the ranking after the control process was as follows: RCAFL, RCAMax, and finally, CDFL. Although the lower fatigue resistance can be explained in the RCAMax sample by the brittleness of the RCA coarse aggregates (Bhusal and Wen 2013), this is not so clear with the RCA and C&D filler, where fatigue life was reported to be improved (Chen et al. 2011). This could then be attributed to either the RCA sources in the different studies having inconsistencies or the differences with the control not being significant enough to make a conclusion one way or the other. The similar performance of the RCAFL mixture to the control in MMLS3 cracking suggests the latter explanation.

Besides the testing of the waste fillers, this study also advanced the practice of evaluating crack resistance with MMLS3, which is a challenge to observe due the critical part of the phenomenon occurring on a microscopic scale. The vertical deformation showed good correlation with the estimated crack length from DIC. The inflection in the crack length that occurs during sample failure seems to lag by a few hundred cycles after the same inflection in the vertical deformation.

Conclusions

The current paper looks at the mechanical cracking behavior of SDA with waste filler replacement implementing a multiscale approach using IT stiffness and fatigue tests along with the MMLS3 cracking test and DIC analysis. The following conclusions can be drawn:

- The replacement of RCA filler in SDA asphalt resulted in a somewhat lower stiffness, but was found to be similar in fatigue and cracking resistance.
- The replacement of RCA coarse aggregate increased the stiffness of the mixture.
- The replacement of C&D filler led to similar stiffness properties but reduced the fatigue resistance.
- The MMLS3 cracking test can be used to monitor the fatigue behavior of asphalt mixtures at larger scales, clearly showing the regions of fatigue, crack propagation and complete failure.
- DIC can be used to monitor the cracking with MMLS3 loading, with sample failure corresponding to crack propagation in the sample. The method used to measure the crack length was effective but could still be improved to reduce the effects of the evaluator.

Although showing marginally lower fatigue resistance at the intermediate scale, control and RCA filler samples showed the same performance at larger scale. The multiscale approach has shown that RCA and C&D waste had no adverse effect on the performances investigated here and these materials can be a viable option for use in asphalt mixtures.

Data Availability Statement

Some or all data, models, or code that support the findings of this study are available from the corresponding author upon reasonable request.

Acknowledgments

The activity presented in this paper is part of the Swiss National Science Foundation (SNF) Grant No. 205121_178991/1 for the project titled "Urban Mining for Low Noise Urban Roads and Optimized Design of Street Canyons." Thanks are given to the Empa 308 Concrete and Asphalt Lab technical staff for performing a part of the sample preparation and testing. Thanks are also given to FAMSA (Massongex, Switzerland) for providing the asphalt mixture materials and FBB (Hinwil, Switzerland) for providing the RCA and binder.

References

Albayati, A., Y. Wang, Y. Wang, and J. Haynes. 2018. "A sustainable pavement concrete using warm mix asphalt and hydrated lime treated recycled concrete aggregates." *Sustainable Mater. Technol.* 18: e00081. https://doi.org/10.1016/j.susmat.2018.e00081.

Arabani, M., and A. R. Azarhoosh. 2012. "The effect of recycled concrete aggregate and steel slag on the dynamic properties of asphalt mixtures." *Constr. Build. Mater.* 35: 1–7. https://doi.org/10.1016/j.conbuildmat.2012.02.036.

Arraigada, M., A. Pugliessi, M. N. Partl, and F. Martinez. 2014. "Effect of full-size and down-scaled accelerated traffic loading on pavement behavior." *Mater. Struct.* 47: 1409–1424. https://doi.org/10.1617/s11527-014-0319-2.

Bhusal, S., and H. Wen. 2013. "Evaluating recycled concrete aggregate as hot mix asphalt aggregate." *Adv. Civ. Eng. Mater.* 2 (1): 252–265. https://doi.org/doi:10.1520/ACEM20120053.

Bühlmann, E., and E. Hammer. 2017. "Towards semi-dense asphalt mixtures that guarantee acoustic performance and durability." In *Proc., Internoise 2017*. Petaluma, CA: Institute of Noise Control Engineering.

CEN (European Committee for Standardization). 2002. *Bituminous mixtures—Test method for hot mix asphalt—Part 29: Determination of the dimensions of bituminous specimen*. EN 12697-29. Brussels, Belgium: CEN.

CEN (European Committee for Standardization). 2013. *Tests for mechanical and physical properties of aggregates—Part 6: Determination of particle density and water absorption*. EN 1097-6. Brussels, Belgium: CEN.

CEN (European Committee for Standardization). 2015. *Bitumen and bituminous binders. Determination of needle penetration*. EN 1426. Brussels, Belgium: CEN.

CEN (European Committee for Standardization). 2019. *Bituminous mixtures—Test methods—Part 5: Determination of the maximum density.* EN 12697-5. Brussels, Belgium: CEN.

Chen, M., J. Lin, and S. Wu. 2011. "Potential of recycled fine aggregates powder as filler in asphalt mixture." *Constr. Build. Mater.* 25: 3909–3914. https://doi.org/10.1016/j.conbuildmat.2011.04.022.

Di Benedetto, H., C. de La Roche, H. Baaj, A. Pronk, and R. Lundström. 2004. "Fatigue of bituminous mixtures." *Mater. Struct.* 37: 202–216. https://doi.org/10.1007/BF02481620.

EAPA (European Asphalt Pavement Association). 2018. *Asphalt in figures 2017*. Brussels, Belgium: EAPA.

FGSV (Forschungsgesellschaft für Straßen- und Verkehrswesen). 2009. *Arbeitsanleitung zur Bestimmung des Steifigkeits- und Ermuedungsverhaltens von Asphalten mit dem Spaltzug-Schwellversuch als Eingangsgroesse in die Dimensionierung. Forschungsgesellschaft für Straßen- und Verkehrswesen*. Köln, Germany: FGSV.

Gauch, M., C. Matasci, I. Hincapié, R. Hörler, and H. Böni. 2016. *Material- und Energieressourcen sowie Umweltauswirkungen der baulichen Infrastruktur der Schweiz*. Rep. No. 21033. St. Gallen, Switzerland: Empa–Materials Science and Technology.

Kareem, A. I., H. Nikraz, and H. Asadi. 2018. "Evaluation of the double coated recycled concrete aggregates for hot mix asphalt." *Constr. Build. Mater.* 172: 544–552. https://doi.org/10.1016/j.conbuildmat.2018.03.158.

Marie, I., and H. Quiasrawi. 2012. "Closed-loop recycling of recycled concrete aggregates." *J. Cleaner Prod.* 37: 243–248. https://doi.org/10.1016/j.jclepro.2012.07.020.

McGennis, R. B., R. M. Anderson, T. W. Kennedy, and M. Solaimanian. 1995. *Background of SUPERPAVE asphalt mixture design and analysis*. Washington, DC: Federal Highway Administration.

Mikhailenko, P., M. R. Kakar, Z. Piao, M. Bueno, and L. Poulikakos. 2020a. "Incorporation of recycled concrete aggregate (RCA) fractions in semi-dense asphalt (SDA) pavements: Volumetrics, durability and mechanical properties." *Constr. Build. Mater.* 264: 120166. https://doi.org/10.1016/j.conbuildmat.2020.120166.

Mikhailenko, P., Z. Piao, M. R. Kakar, M. Bueno, S. Athari, R. Pieren, K. Heutschi, and L. Poulikakos. 2020b. "Low-noise pavement technologies and evaluation techniques: A literature review." *Int. J. Pavement Eng.* 1–24. https://doi.org/10.1080/10298436.2020.1830091.

Mikhailenko, P., Z. Piao, M. R. Kakar, M. Bueno, and L. D. Poulikakos. 2021. "Durability and surface properties of low-noise pavements with recycled concrete aggregates." *J. Cleaner Prod.* 319: 128788. https://doi.org/10.1016/j.jclepro.2021.128788.

Monier, V., S. Mudgal, M. Hestin, M. Trarieux, and S. Mimid. 2011. *Service contract on management of construction and demolition waste–SR1 final report task 2*. Brussels, Belgium: European Commission.

Nedeljković, M., J. Visser, B. Šavija, S. Valcke, and E. Schlangen. 2021. "Use of fine recycled concrete aggregates in concrete: A critical review." *J. Build. Eng.* 38: 102196. https://doi.org/10.1016/j.jobe.2021.102196.

Ossa, A., J. L. García, and E. Botero. 2016. "Use of recycled construction and demolition waste (CDW) aggregates: A sustainable alternative for the pavement construction industry." *J. Cleaner Prod.* 135: 379–386. https://doi.org/10.1016/j.jclepro.2016.06.088.

Piao, Z., P. Mikhailenko, M. R. Kakar, M. Bueno, S. Hellweg, and L. D. Poulikakos. 2021. "Urban mining for asphalt pavements: A review." *J. Cleaner Prod.* 280: 124916. https://doi.org/10.1016/j.jclepro.2020.124916.

Poulikakos, L. D., S. dos Santos, M. Bueno, S. Kuentzel, M. Hugener, and M. N. Partl. 2014. "Influence of short and long term aging on chemical, microstructural and macro-mechanical properties of recycled asphalt mixtures." *Constr. Build. Mater.* 51: 414–423. https://doi.org/10.1016/j.conbuildmat.2013.11.004.

Swiss Standard. 2013. *Semidichtes Mischgut und Deckschichten Festlegungen*. SN 640 436. Zürich. Switzerland: Normierungsorganisation im Strassen- und Verkehrswesen der Schweiz.

Wu, S., B. Muhunthan, and H. Wen. 2017. "Investigation of effectiveness of prediction of fatigue life for hot mix asphalt blended with recycled concrete aggregate using monotonic fracture testing." *Constr. Build. Mater.* 131: 50–56. https://doi.org/10.1016/j.conbuildmat.2016.11.045.

Zaumanis, M., M. Arraigada, and L. D. Poulikakos. 2020. "100% recycled high-modulus asphalt concrete mixture design and validation using vehicle simulator." *Constr. Build. Mater.* 260: 119891. https://doi.org/10.1016/j.conbuildmat.2020.119891.

Zaumanis, M., M. Arraigada, S. A. Wyss, K. Zeyer, M. C. Cavalli, and L. D. Poulikakos. 2019. "Performance-based design of 100% recycled hot-mix asphalt and validation using traffic load simulator." *J. Cleaner Prod.* 237: 117679. https://doi.org/10.1016/j.jclepro.2019.117679.